Science
AAAS

Varying planetary heat sink led to global-warming slowdown and acceleration

Xianyao Chen and Ka-Kit Tung

Science **345**, 897 (2014);
DOI: 10.1126/science.1254937

Science (print ISSN 0036-8075; online ISSN 1095-9203) is published weekly, except the last week in December, by the American Association for the Advancement of Science, 1200 New York Avenue NW, Washington, DC 20005.

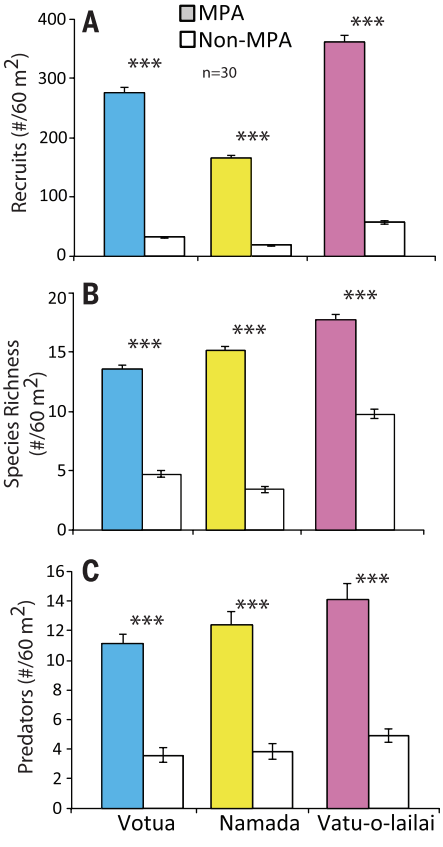

Fig. 5. Density and species richness of fish recruits, and density of predators, in MPAs and non-MPAs. (**A**) Density (±SE) and (**B**) species richness of recruits. (**C**) Density of predators. n = 30 transect per site. $P < 0.001$ for all contrasts.

the recovery of more-degraded habitats (*34*). However, export to degraded reefs will be constrained if recruits avoid chemical cues from degraded reefs. In some locations, export occurs (*35*), but in other areas, there is minimal connectivity, even between protected and exploited populations separated by small distances (*36*). These divergent outcomes could occur if intact reefs export larvae to similar communities but not to degraded, seaweed-dominated communities. The protected and fished areas we studied differ in coral cover, seaweed cover, herbivory rates, and biomass of herbivorous fishes (*9*). Thus, organisms settling only 100 m apart experience dramatically different environments. Our findings suggest that once degradation passes some critical but as yet undetermined threshold, recruit behavior may constrain the value of healthy reefs as larval sources for populations in degraded habitats.

To produce the desired connections between healthy reefs as a source of larvae and degraded reefs as targeted settlement sites where recruitment can promote reef resilience, managers will have to suppress the chemical barrier produced by seaweeds and enhance the chemical "call" of corals and CCA. A promising strategy could be to reduce the harvest of critical species of herbivorous fishes beyond MPA borders. Feeding by specific mixes of these fishes can remove seaweeds, enhance CCA, enhance corals (*6*, *9*, *12*, *33*), and replace chemical cues of degradation with chemical stimulants for recruitment.

REFERENCES AND NOTES

1. L. Alvarez-Filip, N. K. Dulvy, J. A. Gill, I. M. Côté, A. R. Watkinson, *Proc. Biol. Sci.* **276**, 3019–3025 (2009).
2. N. A. J. Graham, K. L. Nash, *Coral Reefs* **32**, 315–326 (2013).
3. T. A. Gardner, I. M. Côté, J. A. Gill, A. Grant, A. R. Watkinson, *Science* **301**, 958–960 (2003).
4. J. F. Bruno, E. R. Selig, *PLOS ONE* **2**, e711 (2007).
5. T. P. Hughes, N. A. J. Graham, J. B. C. Jackson, P. J. Mumby, R. S. Steneck, *Trends Ecol. Evol.* **25**, 633–642 (2010).
6. D. E. Burkepile, M. E. Hay, *Proc. Natl. Acad. Sci. U.S.A.* **105**, 16201–16206 (2008).
7. P. J. Mumby, R. S. Steneck, *Trends Ecol. Evol.* **23**, 555–563 (2008).
8. A. J. Cheal *et al.*, *Coral Reefs* **29**, 1005–1015 (2010).
9. D. B. Rasher, A. S. Hoey, M. E. Hay, *Ecology* **94**, 1347–1358 (2013).
10. S. K. Wilson *et al.*, *Conserv. Biol.* **26**, 995–1004 (2012).
11. M. Nyström *et al.*, *Ecosyst.* **15**, 695–710 (2012).
12. T. P. Hughes *et al.*, *Curr. Biol.* **17**, 360–365 (2007).
13. A. J. Cheal, M. Emslie, M. A. MacNeil, I. Miller, H. Sweatman, *Ecol. Appl.* **23**, 174–188 (2013).
14. H. Cesar, L. Burke, L. Pet-Soede, *The Economics of World Wide Coral Reef Degradation* (Cesar Environmental Economics Consulting, Netherlands, 2003).
15. I. B. Kuffner, V. J. Paul, *Coral Reefs* **23**, 455–458 (2004).
16. H. Watanabe, T. Fujisawa, T. W. Holstein, *Dev. Growth Differ.* **51**, 167–183 (2009).
17. Y. Benayahu, Y. Loya, *Bull. Mar. Sci.* **31**, 514–522 (1981).
18. T. R. McClanahan, R. Arthur, *Ecol. Appl.* **11**, 559–569 (2001).
19. D. F. Gleason, B. S. Danilowicz, C. J. Nolan, *Coral Reefs* **28**, 549–554 (2009).
20. Y. Golbuu, R. H. Richmond, *Mar. Biol.* **152**, 639–644 (2007).
21. L. Harrington, K. Fabricius, G. De'ath, A. Negri, *Ecology* **85**, 3428–3437 (2004).
22. J. Tebben *et al.*, *PLOS ONE* **6**, e19082 (2011).
23. S. N. Arnold, R. S. Steneck, *PLOS ONE* **6**, e28681 (2011).
24. J. Atema, M. J. Kingsford, G. Gerlach, *Mar. Ecol. Prog. Ser.* **241**, 151–160 (2002).
25. D. B. Rasher, E. P. Stout, S. Engel, J. Kubanek, M. E. Hay, *Proc. Natl. Acad. Sci. U.S.A.* **108**, 17726–17731 (2011).
26. T. D. Andras *et al.*, *J. Chem. Ecol.* **38**, 1203–1214 (2012).
27. D. L. Dixson, M. S. Pratchett, P. L. Munday, *Anim. Behav.* **84**, 45–51 (2012).
28. J. M. Leis, U. Siebeck, D. L. Dixson, *Integr. Comp. Biol.* **51**, 826–843 (2011).
29. D. Lecchini, V. P. Waqalevu, E. Parmentier, C. A. Radford, B. Banaigs, *Mar. Ecol. Prog. Ser.* **475**, 303–307 (2013).
30. G. Gerlach, J. Atema, M. J. Kingsford, K. P. Black, V. Miller-Sims, *Proc. Natl. Acad. Sci. U.S.A.* **104**, 858–863 (2007).
31. A. H. Baird, M. S. Pratchett, A. S. Hoey, Y. Herdiana, S. J. Campbell, *Coral Reefs* **32**, 803–812 (2013).
32. M. S. Pratchett, D. McCowan, J. A. Maynard, S. F. Heron, *PLOS ONE* **8**, e70443 (2013).
33. S. M. Lewis, *Ecol. Monogr.* **56**, 183–200 (1986).
34. P. F. Sale *et al.*, *Trends Ecol. Evol.* **20**, 74–80 (2005).
35. H. B. Harrison *et al.*, *Curr. Biol.* **22**, 1023–1028 (2012).
36. S. R. Palumbi, *Annu. Rev. Environ. Resour.* **29**, 31–68 (2004).

ACKNOWLEDGMENTS

Support was provided by NSF grant OCE-0929119, NIH grant U01-TW007401, and the Teasley Endowment. We thank V. Bonito for assistance and the Fijian government and the Korolevu-i-wai district elders for research permissions. Data are tabulated in the supplementary materials.

SUPPLEMENTARY MATERIALS

www.sciencemag.org/content/345/6199/892/suppl/DC1
Materials and Methods
Fig. S1
Tables S1 to S4
References (*37*–*42*)

21 April 2014; accepted 23 June 2014
10.1126/science.1255057

CLIMATE

Varying planetary heat sink led to global-warming slowdown and acceleration

Xianyao Chen[1,2] and Ka-Kit Tung[2]*

A vacillating global heat sink at intermediate ocean depths is associated with different climate regimes of surface warming under anthropogenic forcing: The latter part of the 20th century saw rapid global warming as more heat stayed near the surface. In the 21st century, surface warming slowed as more heat moved into deeper oceans. In situ and reanalyzed data are used to trace the pathways of ocean heat uptake. In addition to the shallow La Niña–like patterns in the Pacific that were the previous focus, we found that the slowdown is mainly caused by heat transported to deeper layers in the Atlantic and the Southern oceans, initiated by a recurrent salinity anomaly in the subpolar North Atlantic. Cooling periods associated with the latter deeper heat-sequestration mechanism historically lasted 20 to 35 years.

Increasing anthropogenic greenhouse-gas emissions perturb Earth's radiative equilibrium, leading to a persistent imbalance at the top of the atmosphere (TOA) despite some longwave radiative adjustment. Energy balance requires that this TOA imbalance for the planet equal the time rate of increase of the total heat content in the atmosphere-ocean system (*1*). Because the heat capacity of the atmosphere and the cryosphere is small, about 90% of the total heat content is in the form of ocean heat content (OHC) (*2*, *3*). Although the magnitude of the TOA

[1]Key Laboratory of Physical Oceanography, Ocean University of China, Qingdao, China. [2]Department of Applied Mathematics, University of Washington, Seattle, WA, USA.
***Corresponding author. E-mail: ktung@uw.edu**

radiative imbalance is uncertain, variously estimated (*1*, *2*, *4*) at 0.5 to 1.0 W m^{-2}, its sign is believed to be positive on multiyear time scales; therefore, this forced total OHC should be increasing monotonically over longer periods even through the current period of slowed warming (*5*, *6*). In fact, that expectation is verified by observation (red curve in Fig. 1A, which is an approximation to the total OHC). What the extent of radiative forcing does not determine, though, is OHC's vertical distribution, which is controlled by the ocean's internal variability, with each ocean basin having its own characteristic time scale. And it is the vertical distribution that is important in determining the sea-surface temperature (SST), given how voluminous the ocean column is.

The current period of global-warming slowdown coincidently occurred during the era of Argo profiling floats (*7*), which were gradually deployed since the end of the 20th century and achieved near-global coverage of the world's oceans by 2005. Before that milestone, other data types, such as the expendable bathythermographs, were available but contained depth bias. After its recent correction (*8*–*10*), the largest remaining uncertainty, related to the infilling of the undersampled areas, especially in the Southern Ocean, was estimated to be less than 0.05×10^{23} J since 1993 by Lyman and Johnson (*11*) for the global mean. Monthly objectively analyzed subsurface temperature and salinity at 24 levels in the upper 1500 m, called the Ishii data (*10*, *12*, *13*), were used in this study (supplementary materials). Data below 2000 m are very sparse, but are probably not needed for our purpose of revealing recent signals from above.

Observed SST and OHC

The global-mean temperature in the first decade of the 21st century has very little trend (*6*, *14*), in contrast to the latter part of the 20th century, which saw rapid global warming (*2*). Figure 1A shows that, in the 21st century, the global-mean SST warming rate has slowed to almost zero for more than a decade—called a slowdown or hiatus—with short-term El Niño–Southern Oscillation (ENSO)–like variation superimposed on it. Thus, two time scales are seen: a

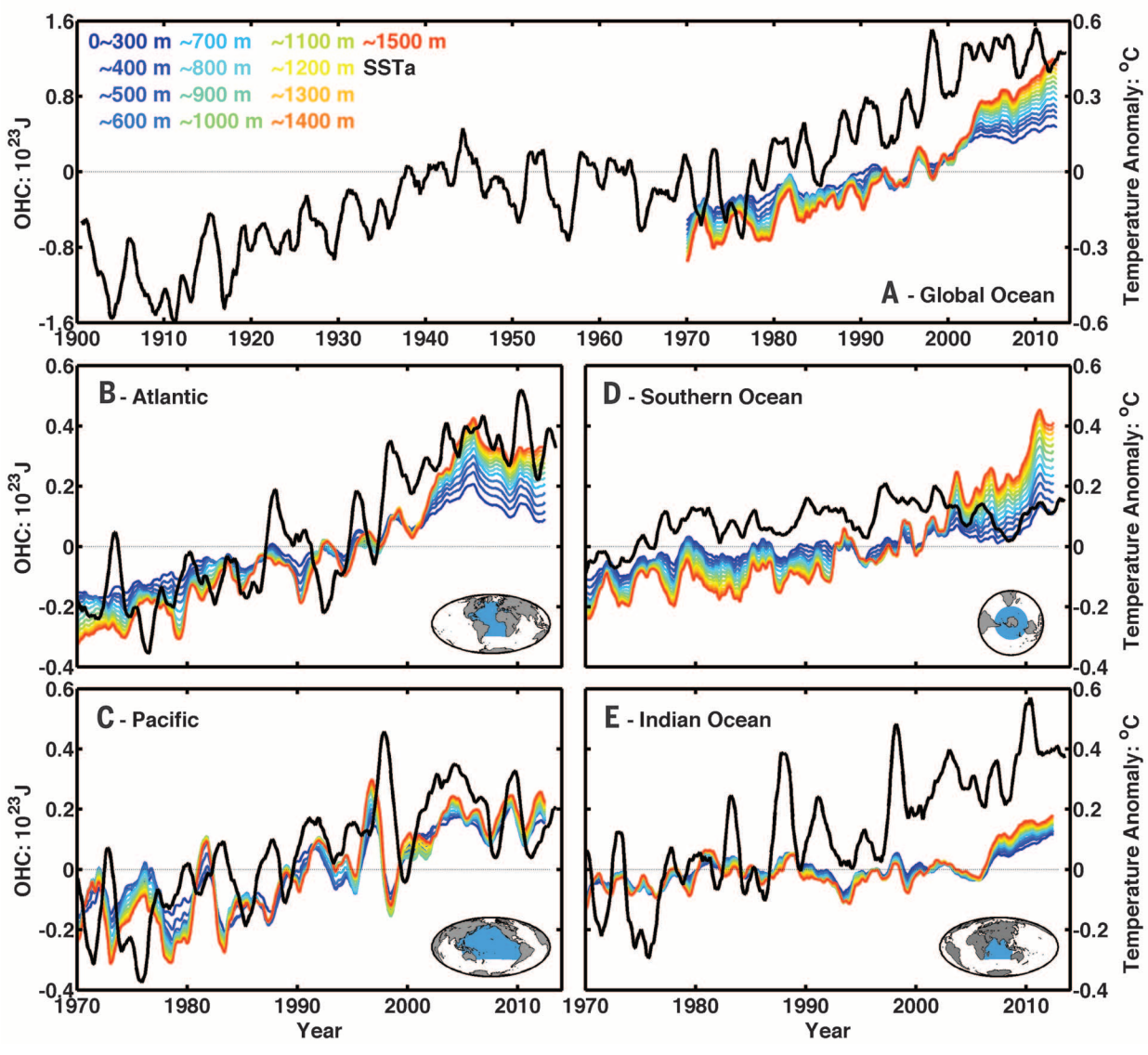

Fig. 1. Integrated OHC. Integrated from the surface to different indicated depths in the global ocean (**A**), the Atlantic (**B**), the Pacific (**C**), the Southern Ocean (**D**), and the Indian Ocean (**E**). Shown is the 12-month running mean deviation from the climatological mean (1970 to 2012) for each layer, so attention should not be focused on the absolute distance between the curves but should be on their relative changes in time. Color lines show the OHC in the left scale, in units of 10^{23} J. The black line shows the mean SST up to 2013. (Insets) The division of the globe into the Pacific, the Atlantic, the Indian Ocean, and the Southern Ocean. Although shown in the figure, data in the earlier decades were not as reliable (see Data and Materials and Methods); the discussion in the text is focused on the better-observed regions and periods.

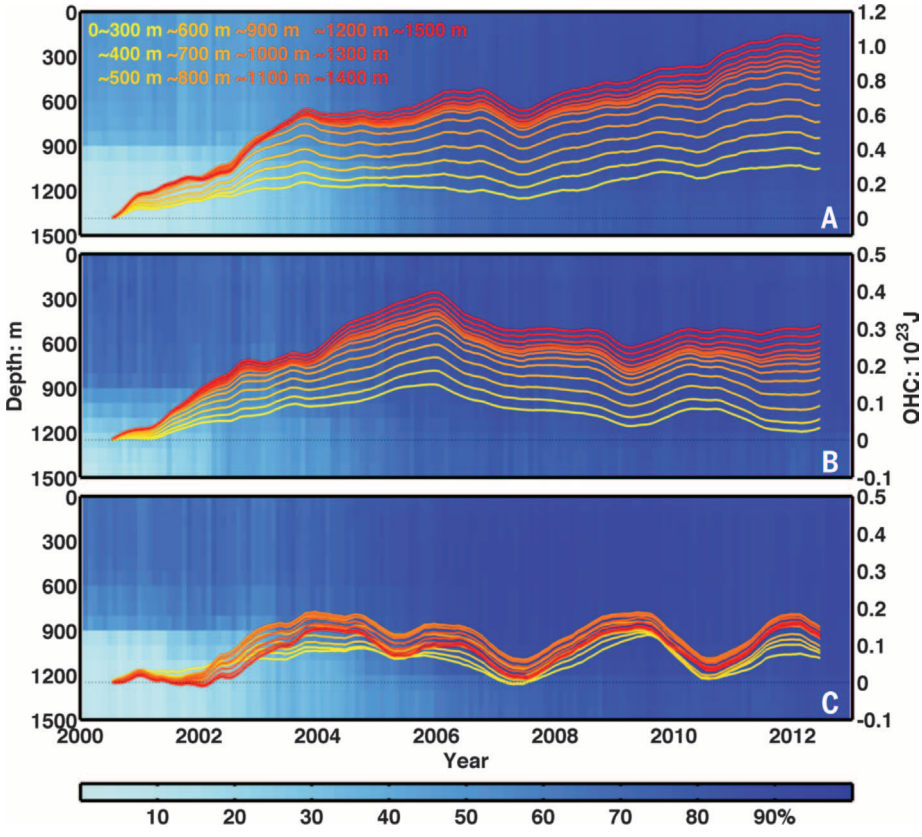

Fig. 2. In situ data coverage in 5°-by-5° grid as a percentage of full coverage. Shown as background blue color shades at each depth as indicated by the axis on the left. Integrated OHC from the surface to each depth (lines with red to yellow colors) for global (**A**), Atlantic (**B**), and Pacific (**C**) oceans are superimposed, with magnitude scale on the right axis. No climatology is removed; all values refer to difference from their 2000 values.

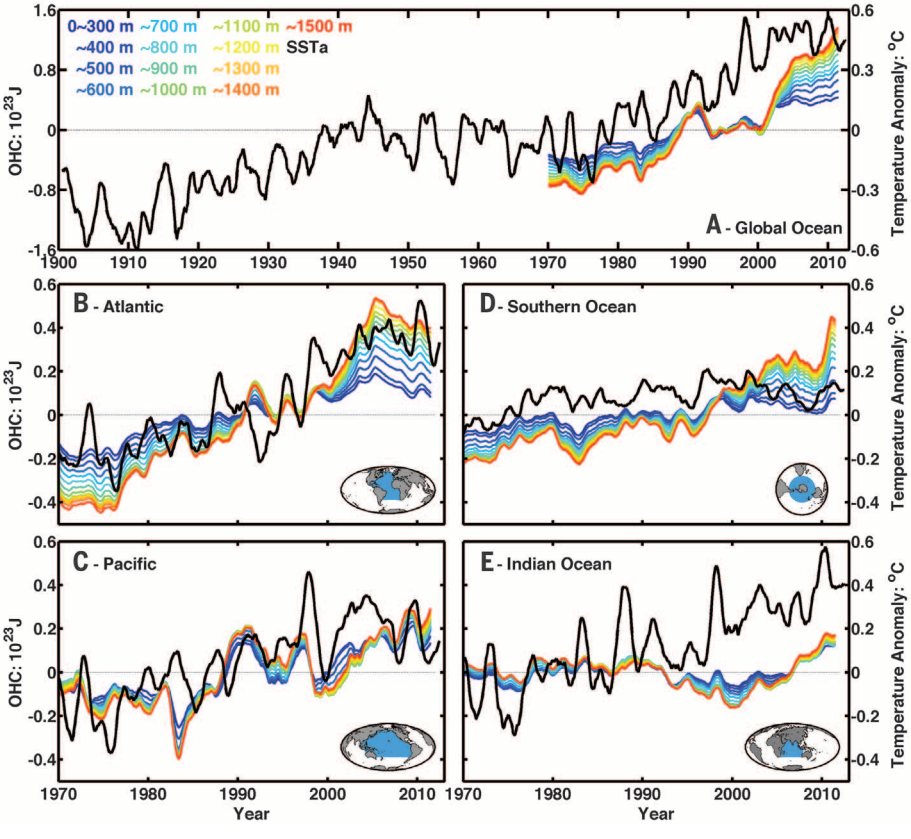

Fig. 3. ORAS4 reanalysis. (**A** to **E**) Same as Fig. 1 except with use of ORAS4 data.

multidecadal nonlinear trend with periods of accelerated warming separated by periods of slowdown and a shorter 2- to 7-year ENSO time scale. We argue that they are caused by different mechanisms.

During the current hiatus, radiative forcing at the TOA by the increasing greenhouse-gas concentration in the atmosphere produces additional warming in deeper and deeper ocean layers. This deepening warming is seen in Fig. 1A, calculated by using the in situ Ishii data (*10*), as an increasing fanning out of the OHC curves (integrated from the surface to different depths) after 1999. Globally, an additional 0.69×10^{23} J has been sequestered since 1999 in the 300- to 1500-m layer by 2012 (Fig. 1A), which, if absent, would have made the upper 300 m warm as fast as the upper 1500 m since 1999. Because the latter has an uninterrupted positive trend, there would have been no slowdown of the warming of the surface or the upper layers. Therefore, the enhanced ocean heat sink is the main cause for the current slowing in surface warming. One can also see from Fig. 1A that there has not been a major reduction in TOA radiative imbalance, as inferred from an absence of a noticeable downward bent in slope in the red curve on multiyear time scales. In the prior two decades, 1980 to 2000, we have the contrasting situation of accelerating surface warming while little additional heat (over the climatological mean) went into the deeper layers. Most of the added heat stayed near the surface, as seen by

the distance between all OHCs integrated from the surface to different depths changing little in time.

Figure 1, B to E, shows that during the 21st century the increased OHC penetration below 300 m occurs mainly in two ocean basins: the Atlantic and the Southern oceans, each accounting for slightly less than half of the global energy storage change since 1999 at those depths. The Pacific shows very little change in the spreading of OHC with depth between the two periods. This recent contrast between the Pacific and the Atlantic is deemed reliable because these are the two basins with adequate data coverage [over 80% on 5°-by-5° grids (Fig. 2)]. A separate analysis of Ocean Reanalysis System 4 (ORAS4) (*15*) data, shown in Fig. 3, verifies the in situ result here (*10*). The reanalysis uses a model to assimilate all forms of observational data and dynamically interpolates across periods of sparse coverage. Although barely noticeable, ORAS4 does have slightly more heat sequestration in the 300 to 700 m in the Pacific since 2001 compared with the Ishii data during the current hiatus period. Nevertheless, neither data set supports the model result of Meehl *et al.* (*5*) that the heat uptake in this layer in the Pacific dominates over other ocean basins during hiatus periods.

The 1997/98 El Niño released a large amount of heat, about 0.42×10^{23} J, from the upper 300 m of the Pacific Ocean to the atmosphere to be radiated as outgoing long-wave radiation. The deeper ocean was not involved, as seen by the OHC curve of the upper 1500 m tracking closely the upper 300-m content in Fig. 1C. Therefore, the time scale was short, and the upper 300 m recovered 3 to 4 years later. The 1982 El Niño also released a large amount of heat from the upper 300 m of the Pacific but did not "trigger" a period of slowdown in global surface warming.

Over the whole globe, the dominant spatial mode of variability in OHC in the upper 300 m [as shown by the first empirical orthogonal function (EOF), which explains the most variance], occurs mainly in the tropical Pacific and has the structure of ENSO variability (Fig. 4, A and B). Figure 4, E and F, shows the time series [called the principal components (PC)] associated with these EOFs. The spatial pattern of the upper 300 m resembles that associated with La Niña in the current period, because the blue PC1 changes to negative around year 2000. The leading pattern is very similar to the La Niña pattern in the SST (fig. S1A), and their PC1s are almost the same (fig. S1I). The prevalence of La Niña, with the associated shallow subduction of heat below the surface in the Pacific, has been proposed as the reason for the current hiatus (*16*). However, our result shows that the change in heat storage under the Pacific is not nearly enough to compensate for the surface hiatus—the entire upper 300 m is itself in a net La Niña phase. Figure 4, C and D, shows that the dominant OHC variability below 300 m occurs mainly in the Atlantic basin and the Antarctic Circumpolar Current (ACC) region. This combined warming pattern in the lower layer became positive toward the end of the 20th century, after two decades with very little heat uptake anomaly below 300 m (see the red PC1). The Atlantic initiated the heat sequestration toward the end of the 20th century below 700 m. Indian Ocean's deeper layers warmed last and with much smaller amplitude. Figure S1 shows these results in finer vertical resolution, whereas fig. S2 reproduces these results by using ORAS4 data.

In the Southern Ocean, the largest warming below 300 m occurs in the ACC region (*17*, *18*), in the Atlantic sector, diminishing in amplitude as the current flows eastward (Fig. 4C), first to the Indian Ocean and then to the Pacific. During the current 14 years, the 300- to 1500-m layer of the North and South Atlantic together contributed

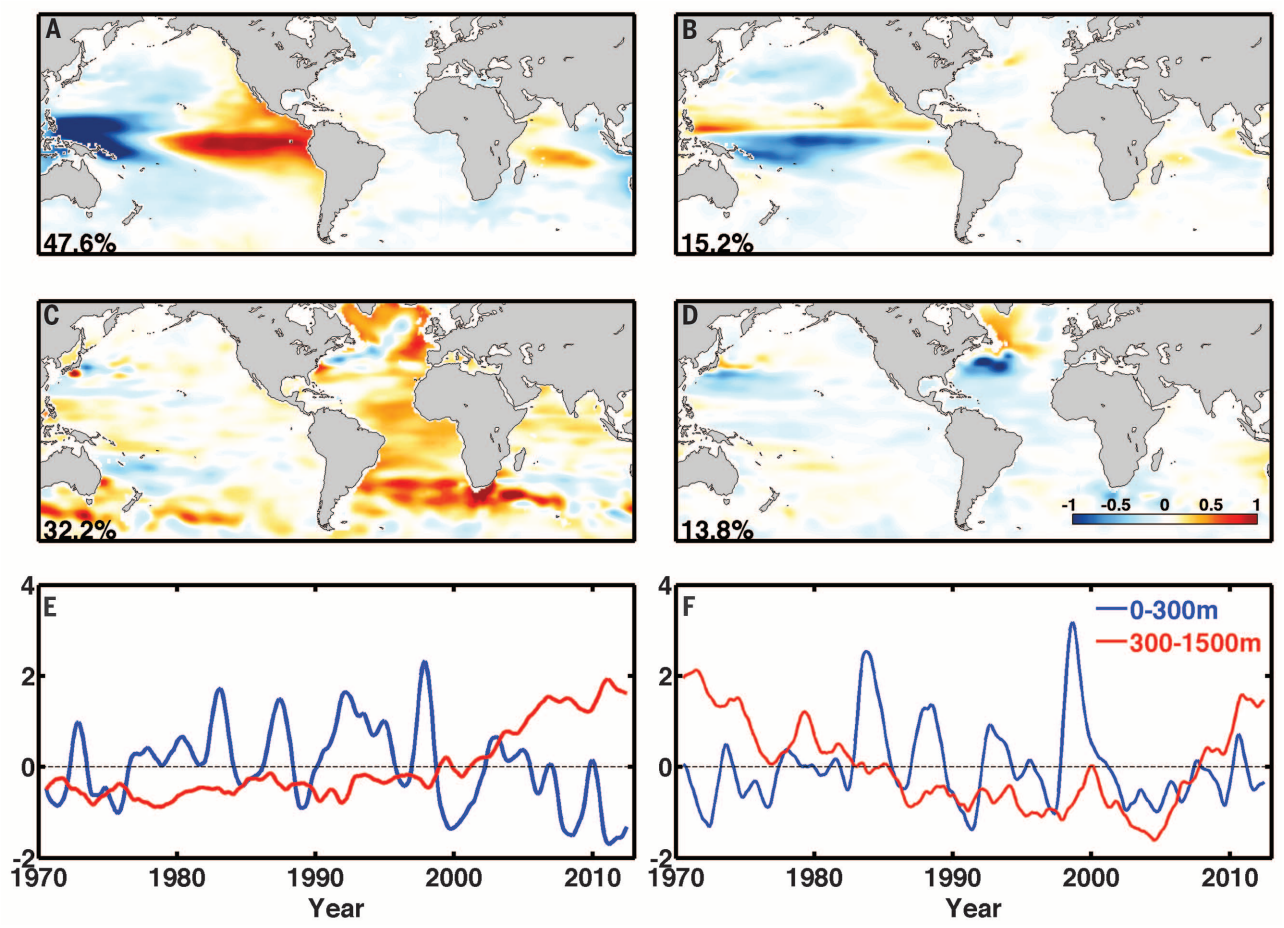

Fig. 4. EOF of the global oceans. The first (left column) and second (right column) EOF modes of the OHC in the layers 0 to 300 m (**A** and **B**) and 300 to 1500 m (**C** and **D**), respectively, in the same unit of 10^{19} J. (**E** and **F**) The PC time series associated with each EOF mode (blue for the upper layer and red for the lower layer). The PCs have been normalized by the standard deviation, which is multiplied to the EOF modes. The percentage of variance explained by each EOF is indicated in each EOF panel. Because the second EOF is small, attention should be focused on the first EOF.

0.16 ± a standard deviation of 0.03 W m^{-2} (per Earth's area) to the global mean of 0.30 ± 0.04 W m^{-2}, slightly more than the rest of the global oceans combined. [The global value for the entire 0 to 1500 m in the Ishii data is 0.49 ± 0.05 W m^{-2}.]

Over a meridional section (Fig. 5, A and B) of OHC across the Atlantic basin, there was a dramatic and broad shift in how heat penetrated all the way to 1500 m in mid- to high-latitude North Atlantic in 1999 to 2012 relative to the prior decades. The detrended version is shown in fig. S3; the spatial pattern in the North Atlantic is consistent with a change of the thermohaline circulation (*19*, *20*). There is a "dipole" meridional pattern near the 200-m depth under a "monopole" SST warming, similar to the pattern generated by regressing the data onto either the Atlantic Meridional Overturning (AMO) index (*21*, *22*) or the detrended tropical North Atlantic SST, known from model "water hosing" experiments to be a manifestation of variations in the Atlantic Meridional Overturning Circulation (AMOC) (*22*). The spatial pattern of this possibly recurring internal variability can be seen in the longer records shown in fig. S4, although poorer, earlier data are needed to see the previous episode.

In contrast to the Atlantic, the OHC change in the Pacific Ocean occurs within a shallow layer (above 300 m) and mainly in the east-west direction (see Fig. 5, C and D, which are the meridional mean of the Pacific Ocean), similar to that during ENSO events. During the current period, a thin layer of colder surface water overlies a very warm pool of water in the tropical western Pacific, driven by an anomalously strong (westward) trade wind (*23*). The warm water was only slightly displaced downward and can quickly slosh up and eastward when the west trade-wind anomaly relaxes, as suggested by England *et al.* (*23*). The Pacific mean is further broken down into the tropical versus the subtropical Pacific in fig. S5. There is some indication of heat subduction by the subtropical cell, as previously proposed (*23*, *24*), but the magnitude is small and does not affect the Pacific mean shown in Fig. 5C.

The salinity mechanism

A mechanism that can account for the speed with which heat penetrates to such great depths is deep convection caused by vertical density differences. Salinity changes at subpolar North Atlantic are known to affect deep-water formation to initiate such an ocean circulation shift (*25*). The salinity there (Fig. 6A) shifted to a positive anomaly that penetrated vertically to 1500 m very rapidly in the 21st century, reaching historically high values since measurements began (*26*). This is in contrast to the negative anomaly during the prior three decades, when surface warming was rapid. Because the ocean data were less sparse in the North Atlantic, we extend the plot back to 1950 and reveal that the salinity anomaly was also positive before 1970, during another episode of surface hiatus. These salinity shifts correspond well in timing to the OHC shifts (Fig. 6B), which are also coincident with surface transitions from global-warming slowdown to rapid warming and then to the current slowdown, with intervals between shifts lasting about three decades. Curry *et al.* (*27*) reported a freshening of the subpolar North Atlantic waters from the 1950s to 1990s and cited global warming as one of the reasons. However, over the longer period reported here, there was very little trend in the salinity, only a vacillating cycle.

There is no accepted single theory, but theoretical explanations of these vacillating regime shifts mostly involve variations of the AMOC (*20*, *25*). Because of excessive evaporation, tropical surface water is more saline. A faster AMOC tends to transport more saline water to the North Atlantic subpolar region, where it loses some heat to the cold atmosphere and sinks. The heat from the transported tropical water tends to melt more ice (*20*), which makes the surface water in the subpolar regions less dense. These two effects oppose each other. Eventually the fresh water from ice melts wins out. The less-dense water then slows the AMOC after a few-years lag (*28*). A slower AMOC then transports less tropical saline water northward, and the opposing phase of the cycle commences. Other versions of the mechanism are also available (*29*, *30*). Because the record for the AMOC strength is short (only since 2004), the above scenario cannot be verified observationally, but it is consistent with the mechanism described by Danabasoglu *et al.* (*31*) as indeed occurring in the Community Climate System Model 4 (CCSM4) (*32*).

Although there is very little trend in the OHC in the subpolar North Atlantic where the salinity-induced vacillation cycle dominates, there is a linear OHC trend equatorward of 45°N and °S in

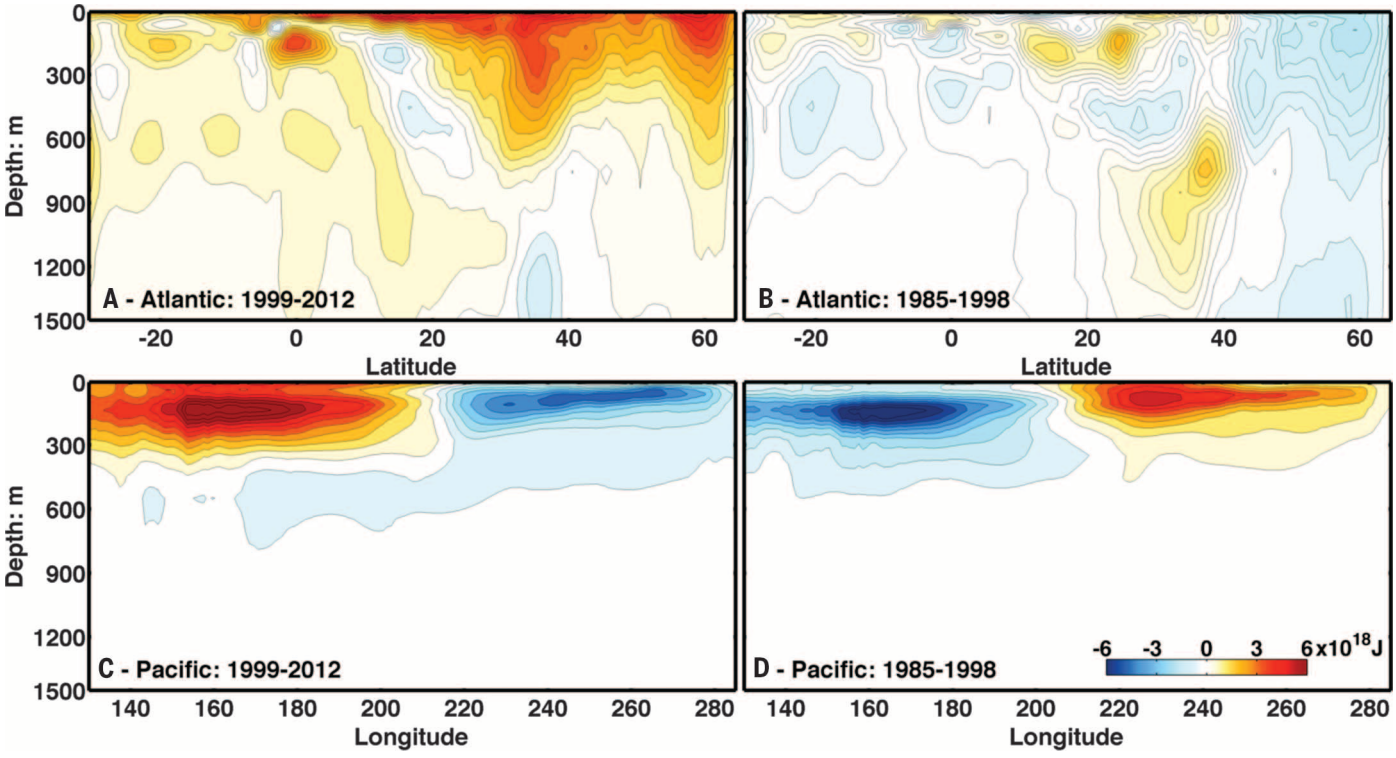

Fig. 5. Contrasting the change in heat content in the Pacific versus the Atlantic. (**A** and **B**) OHC (for each 5-m layer) in the Atlantic basin zonally averaged over the basin as a function of latitude. (**C** and **D**) OHC integrated meridionally (35°S to 65°N) over the Pacific basin as a function of longitude. (A and C) Averaged over the recent 14 years. (B and D) Averaged over the previous 14 years. Not detrended.

the Atlantic basin (including the Southern Ocean) (fig. S6), which is likely anthropogenically forced. This secular increase in OHC is not associated with a corresponding trend in salinity. It reflects mainly the increase in greenhouse heating from above and does not necessarily reflect the speed of the heat transport by the AMOC. In the Pacific, there is again very little heat-uptake trend.

Discussion

Many different explanations for the recent global-warming slowdown have been proposed, but they fall mainly into two categories. The first involves a reduction in TOA radiative forcing: by a decrease in stratospheric water vapor (*33*), an increase in background stratospheric volcanic aerosols (*34*), by 17 small volcano eruptions since 1999 (*35*), increasing coal-burning in China (*36*), the indirect effect of time-varying anthropogenic aerosols (*37*), a low solar minimum (*38*), or a combination of these (*39*). Response to solar cycle changes was found to be small (*40*, *41*). The aerosol cooling should have a signature in subsurface ocean (*42*), and yet it is not seen, perhaps suggesting that the proposed radiative effects may be too small. The second involves ocean heat sequestration: The present work follows the original proposal of Meehl *et al.* (*5*, *24*) regarding global deep-ocean heat sequestration. However, our observational result does not support their Pacific-centric view. The duration of the cooling periods in the CCSM4 model they used is typically 10 years, with one rare 15-year hiatus in 375 years and none over 15 years. The current hiatus already lasted over 15 years using their definition of hiatus as periods with zero trend. Comparing that model with observation, we found that model's Atlantic has too little variability with too high frequency (fig. S7 versus Fig. 6). This artifact appears to be attributable to a new overflow parameterization scheme in CCSM4 in the Denmark Strait and Faroe Bank Channel (*31*).

From another perspective, Wu *et al.* (*43*) showed that the instrumental global-mean surface temperature record since 1850 contains two and a half cycles of a multidecadal variation. Each cycle lasted on average 65 years, consisting of an accelerated warming plus a slowdown period. They showed that the primary location of the multidecadal variability is in the North Atlantic and only secondarily in the Pacific. If this multidecadal variability is indeed related to the variations of the AMOC, then we can infer that the time scale of the latter was also 30 years between regime shifts historically. Tung and Zhou (*41*) showed that these multidecadal cycles exist in the Central England Temperature for the past 353 years, with an average period of 70 years (but could be as short as 40 years), consistent with an earlier study using multiproxy data by Delworth and Mann (*44*). They and Zhang *et al.* (*42*) argued that this oscillation is due to an internal variability and not to anthropogenic aerosol forcing (*37*).

Because the atmosphere and the upper ocean in the equatorial Pacific are intimately coupled, the strong trade winds go hand in hand with the east-west SST gradient generated by the La Niña pattern, known as the Bjerknes feedback. Kosaka and Xie (*16*) proposed that the cold eastern Pacific was key to understanding the current warming hiatus. England *et al.* (*23*) attributed the cold eastern equatorial Pacific to the stronger trade winds for the past 20 years, and the trade wind intensification to the multidecadal negative phase of the Interdecadal Pacific Oscillation (IPO). The IPO, defined using the SST in the Pacific Basin including the ENSO region, describes but does not explain the cold eastern Pacific status.

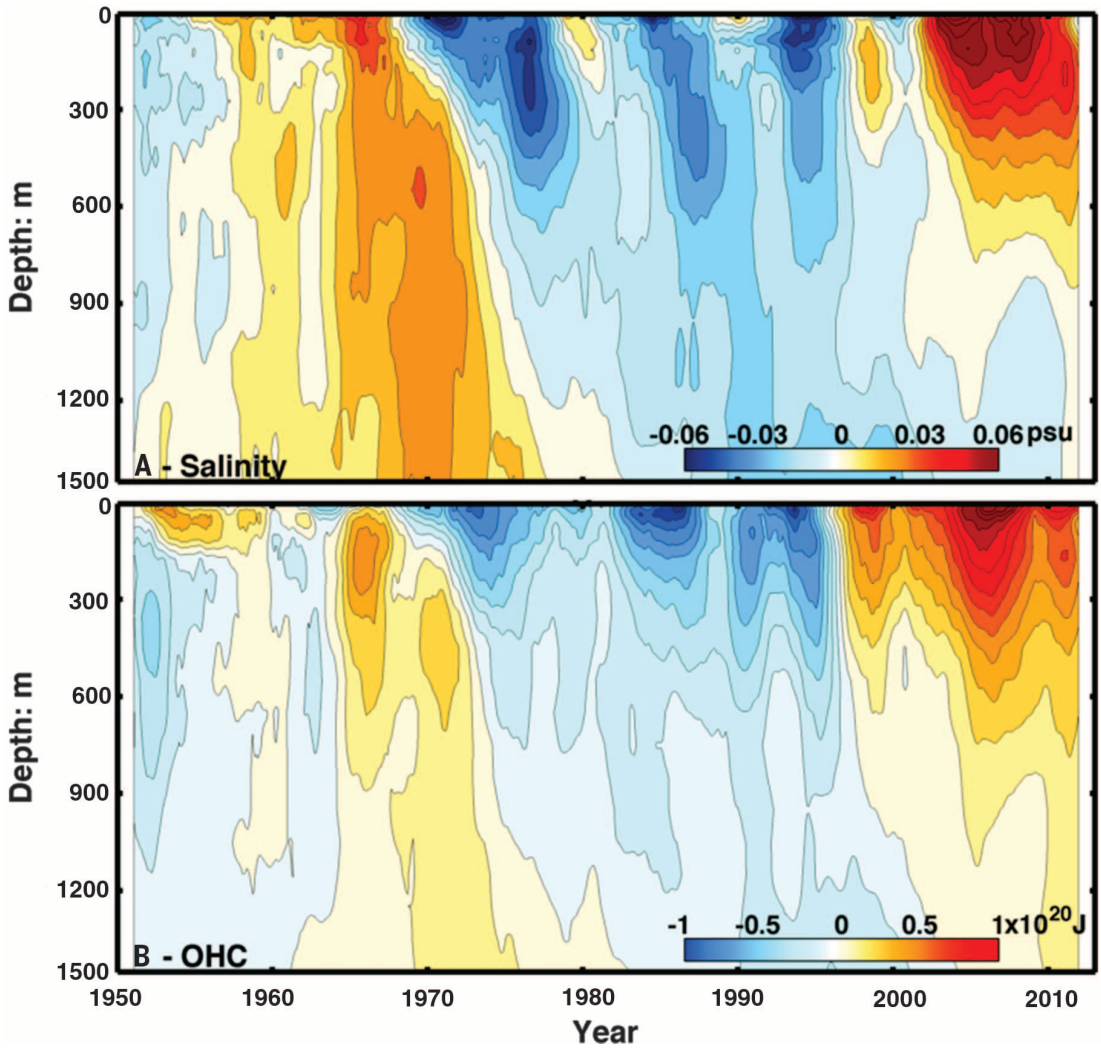

Fig. 6. Climate shifts in salinity and OHC. North Atlantic subpolar (45° to 65°N) mean salinity (A) and 5-m layer OHC (B), 12-month running mean, as a function of years; not detrended, but the climatology for the period 1950 to 2012 was removed.

How could the Pacific SST cool when the heat sink was located in other ocean basins? Why didn't the Atlantic SST simply cool as heat was being subducted in its basin? The Atlantic SST and its upper layers did start to cool (Fig. 1B) after its subpolar salinity peaked and then started to decrease after 2006 (Fig. 6A). Before 2006, our warm salt subduction mechanism does not allow the Atlantic to cool when its subpolar salinity was increasing, because poleward transport of warm salty water and increasing subpolar subduction are parts of the same mechanism of enhanced AMOC upper-ocean transport. During this first part of the hiatus period, the heat deficit must be transferred to other ocean basins, mostly to the Pacific because it is the only other major ocean basin in the Northern Hemisphere, likely through the atmosphere. Zhang and Delworth (*45*) and Zhang *et al.* (*46*) showed by using models that, as the northward heat transport by the AMOC is increased, the atmospheric heat transport decreases in compensation (and vice versa), providing a multidecadal component to the Pacific Decadal Oscillation (PDO). The concept behind the flexible atmospheric heat transport is known as nonlinear baroclinic adjustment (*47*). Thus, almost-"synchronized" hemisphere-wide atmospheric changes are possible (*30*). On climate time scales and from an energy perspective, the amount of radiative energy available to heat the global SST, including the Pacific, is what remains after accounting for the energy sink; it does not matter if the latter is located outside the Pacific.

Conclusion

The fact that the global-mean temperature, along with that of every major ocean basin, has not increased for the past 15 years, as they should in the presence of continuing radiative forcing, requires a planetary sink for the excess heat. Although the tropical Pacific is the source of large interannual fluctuations caused by the exchange of heat in its shallow tropical layer (*3*), the current slowdown is in addition associated with larger decadal changes in the deeper layers of the Atlantic and the Southern oceans. The next El Niño, when it occurs in a year or so, may temporarily interrupt the hiatus, but, because the planetary heat sinks in the Atlantic and the Southern Oceans remain intact, the hiatus should continue on a decadal time scale. When the internal variability that is responsible for the current hiatus switches sign, as it inevitably will, another episode of accelerated global warming should ensue.

REFERENCES AND NOTES

1. K. E. Trenberth, J. T. Fasullo, M. A. Balmaseda, *J. Clim.* **27**, 3129–3144 (2014).
2. Intergovernmental Panel on Climate Change, *Summary for Policymakers, Climate Change 2007: Synthesis Report* (Cambridge Univ. Press, Cambridge, 2007).
3. K. E. Trenberth, J. T. Fasullo, *Earth's Future* **1**, 19–32 (2013).
4. K. E. Trenberth, J. T. Fasullo, *Science* **328**, 316–317 (2010).
5. G. A. Meehl, J. M. Arblaster, J. T. Fasullo, A. Hu, K. E. Trenberth, *Nat. Clim. Change* **1**, 360–364 (2011).
6. D. R. Easterling, M. F. Wehner, *Geophys. Res. Lett.* **36**, L08706 (2009).
7. D. Roemmich *et al.*, *Oceanography* **22**, 46–55 (2009).
8. J. M. Lyman, G. C. Johnson, *J. Clim.* **27**, 1945–1957 (2014).
9. J. M. Lyman *et al.*, *Nature* **465**, 334–337 (2010).
10. M. Ishii, M. Kimoto, *J. Oceanogr.* **65**, 287–299 (2009).
11. J. M. Lyman, G. C. Johnson, *J. Clim.* **21**, 5629–5641 (2008).
12. M. Ishii, A. Shouji, S. Sugimoto, T. Matsuoto, *Int. J. Climatol.* **25**, 865–879 (2005).
13. M. Ishii, M. Kimoto, K. Sakamoto, S. I. Iwasaki, *J. Oceanogr.* **62**, 155–170 (2006).
14. C. A. Katsman, G. J. van Oldenborg, *Geophys. Res. Lett.* **38**, L14610 (2011).
15. M. A. Balmaseda, K. Mogensen, A. T. Weaver, *Q. J. R. Meteorol. Soc.* **139**, 1132–1161 (2013).
16. Y. Kosaka, S.-P. Xie, *Nature* **501**, 403–407 (2013).
17. S. T. Gille, *Science* **295**, 1275–1277 (2002).
18. J. R. Toggweiler, J. Russell, *Nature* **451**, 286–288 (2008).
19. R. Zhang, *Geophys. Res. Lett.* **35**, L20705 (2008).
20. J. Jungclaus, H. Haak, M. Latif, U. Mikolajewicz, *J. Clim.* **18**, 4013–4031 (2005).
21. C. Wang, L. Zhang, *J. Clim.* **26**, 6137–6162 (2013).
22. R. Zhang, *Geophys. Res. Lett.* **34**, L12713 (2007).
23. M. H. England *et al.*, *Nat. Clim. Change* **4**, 222–227 (2014).
24. G. A. Meehl, A. Hu, J. M. Arblaster, J. T. Fasullo, K. E. Trenberth, *J. Clim.* **26**, 7298–7310 (2013).
25. I. V. Polyakov, V. A. Alekseev, U. Bhatt, E. I. Polyakova, X. Zhang, *Clim. Dyn.* **34**, 439–457 (2010).
26. H. Hátún, A. B. Sandø, H. Drange, B. Hansen, H. Valdimarsson, *Science* **309**, 1841–1844 (2005).
27. R. Curry, B. Dickson, I. Yashayaev, *Nature* **426**, 826–829 (2003).
28. M. Dima, G. Lohmann, *J. Clim.* **20**, 2706–2719 (2007).
29. M. G. Wyatt, J. A. Curry, *Clim. Dyn.* **42**, 2763–2782 (2014).
30. M. G. Wyatt, S. Kravtsov, A. A. Tsonis, *Clim. Dyn.* **38**, 929–949 (2012).
31. G. Danabasoglu *et al.*, *J. Clim.* **25**, 5153–5172 (2012).
32. P. R. Gent *et al.*, *J. Clim.* **24**, 4973–4991 (2011).
33. S. Solomon *et al.*, *Science* **327**, 1219–1223 (2010).
34. S. Solomon *et al.*, *Science* **333**, 866–870 (2011).
35. B. D. Santer *et al.*, *Nat. Geosci.* **7**, 185–189 (2014).
36. R. K. Kaufmann, H. Kauppi, M. L. Mann, J. H. Stock, *Proc. Natl. Acad. Sci. U.S.A.* **108**, 11790–11793 (2011).
37. B. B. B. Booth, N. J. Dunstone, P. R. Halloran, T. Andrews, N. Bellouin, *Nature* **484**, 228–232 (2012).
38. J. Hansen, M. Sato, P. Kharecha, K. von Schuckmann, *Atmos. Chem. Phys.* **11**, 13421–13449 (2011).
39. G. A. Schmidt, D. T. Shindell, K. Tsigaridis, *Nat. Geosci.* **7**, 158–160 (2014).
40. J. Zhou, K. K. Tung, *J. Clim.* **23**, 3234–3248 (2010).
41. K. K. Tung, J. Zhou, *Proc. Natl. Acad. Sci. U.S.A.* **110**, 2058–2063 (2013).
42. R. Zhang *et al.*, *J. Atmos. Sci.* **70**, 1135–1144 (2013).
43. Z. Wu, N. E. Huang, J. M. Wallace, B. Smoliak, X. Chen, *Clim. Dyn.* **37**, 759–773 (2011).
44. T. L. Delworth, M. E. Mann, *Clim. Dyn.* **16**, 661–676 (2000).
45. R. Zhang, T. L. Delworth, *Geophys. Res. Lett.* **34**, L23708 (2007).
46. R. Zhang, T. L. Delworth, I. M. Held, *Geophys. Res. Lett.* **34**, L02709 (2007).
47. W. T. Welch, K. K. Tung, *J. Atmos. Sci.* **55**, 1285–1302 (1998).

ACKNOWLEDGMENTS

The research of K.-K.T. is supported by NSF under AGS-1262231. X.C. is supported by Natural Science Foundation of China under 41330960 and 41176029. He thanks First Institute of Oceanography of China for its support during his visit to University of Washington. The authors are grateful to many colleagues and the anonymous reviewers who commented on the manuscript and helped improve it. The data sets used in this study are publicly available in http://rda.ucar.edu/datasets/ds285.3/ and https://climatedataguide.ucar.edu/climate-data/oras4-ecmwf-ocean-reanalysis-and-derived-ocean-heat-content.

SUPPLEMENTARY MATERIALS

www.sciencemag.org/content/345/6199/897/suppl/DC1
Materials and Methods
Data
Figs. S1 to S7
Reference (*48*)

17 April 2014; accepted 11 July 2014
10.1126/science.1254937

REPORTS

QUANTUM OPTICS

All-optical routing of single photons by a one-atom switch controlled by a single photon

Itay Shomroni,* Serge Rosenblum,* Yulia Lovsky, Orel Bechler, Gabriel Guendelman, Barak Dayan†

The prospect of quantum networks, in which quantum information is carried by single photons in photonic circuits, has long been the driving force behind the effort to achieve all-optical routing of single photons. We realized a single-photon–activated switch capable of routing a photon from any of its two inputs to any of its two outputs. Our device is based on a single atom coupled to a fiber-coupled, chip-based microresonator. A single reflected control photon toggles the switch from high reflection (R ~ 65%) to high transmission (T ~ 90%), with an average of ~1.5 control photons per switching event (~3, including linear losses). No additional control fields are required. The control and target photons are both in-fiber and practically identical, making this scheme compatible with scalable architectures for quantum information processing.

Photons are a key player in the growing field of quantum information science. The fact that they do not interact with each other has made them ideal for the communication of quantum information yet has prevented so far the realization of deterministic all-optical quantum gates based on single photons. The difficulty to achieve nonlinear behavior at the level of single photons—namely, photon-photon interactions—is considered a major challenge also in the realization of quantum networks, in which quantum information processing

Department of Chemical Physics, Weizmann Institute of Science, Rehovot 76100, Israel.
*These authors contributed equally to this work. **†Corresponding author. E-mail: barak.dayan@weizmann.ac.il**